

RECENT ADVANCES IN PLASMA CONTROL AND PHYSICS RESEARCH IN THE LARGE HELICAL DEVICE

¹K. TANAKA and ¹LHD experiment group

¹National Institute for Fusion Science, Toki, Japan

Email: tanaka.kenji@nifs.ac.jp

This synopsis summarizes recent advancements in the Large Helical Device (LHD). LHD, the largest superconducting helical system, is equipped with advanced heating and diagnostic tools, facilitating plasma control and physics research. To date, two plasma control techniques have been demonstrated: one utilizing data assimilation (DA) and another involving impurity powder dropping for plasma-wall control. Understanding turbulence characteristics is essential for transport physics. Systematic experiments have clarified turbulence mode transitions and identified notable turbulence characteristics. Additionally, evidence of non-collisional heating by energetic ion driven geodesic acoustic modes has suggested. These achievements represent unique contributions to the development of fusion reactors.

The DA-based control technique combines a data-driven approach, which predicts outcomes from training datasets, with a physics-based model. This technique is highly effective for controlling systems with numerous variables and strongly nonlinear responses, where conventional feedback control is ineffective. Figure 1 illustrates electron cyclotron resonant heating (ECRH) power control using the DA-based technique. Previous transport studies in LHD have established that electron and ion energy transport are governed by gyro-Bohm (GB)-type diffusion. Given that coefficients of GB-type diffusion are initially unknown, they are first determined using training data and then refined using the DA technique. For the control scenario in Fig. 1, training was performed from $t = 0.2$ – 2.2 s. Power balance analyses were conducted every 0.1 s, and at $t = 1.2$ s, the predicted central electron temperature ($T_e(0)$) agreed with its measured value. The target $T_e(0)$ increased linearly from 1.5 keV at $t = 2.2$ s to 4 keV at $t = 4.0$ s, after which it was held constant. DA-based control began at $t = 2.2$ s. The prediction probability function was computed in real time, followed by the estimation of required ECRH power. Subsequently, corresponding control signals were relayed to the ECRH system. Finally, the predicted T_e profiles were assimilated with the measured profiles, and the observed $T_e(0)$ closely matched the target value at $t = 4.0$ s.

Plasma-wall control is a critical issue in fusion research. Impurity powder dropping is a powerful technique for real-time wall control [2]. Previous experiments have demonstrated that B powder improves confinement [2] and increases the density limit. Recent experiments have investigated the effects of Li powder dropping. Figure 2 compares plasma discharges with and without Li powder dropping under identical conditions of line-averaged electron density (\bar{n}_e) and neutral beam (NB) heating power. Panel (a) indicates that the central T_e is approximately 10% higher with Li powder dropping than without it, while panel (b) illustrates that the line-integrated fluctuation amplitude, measured using phase contrast imaging (PCI), is approximately 30% lower with Li powder dropping. A key finding is the effect of Li powder on particle confinement and impurity transport. Figure 2(c) reveals weaker H α and D α intensities in the discharge with Li powder, indicating reduced recycling and improved global particle confinement of bulk ions. Impurity transport was analyzed using impurity pellet injection. Figure 2(d) demonstrates that the decay time of

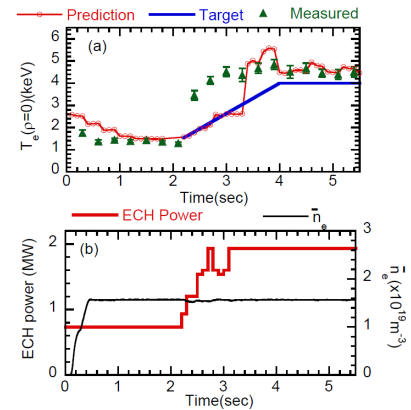


Fig.1 DA-based control of $T_e(0)$. Temporal evolution of (a) $T_e(0)$ and (b) controlled ECRH power and \bar{n}_e [1].

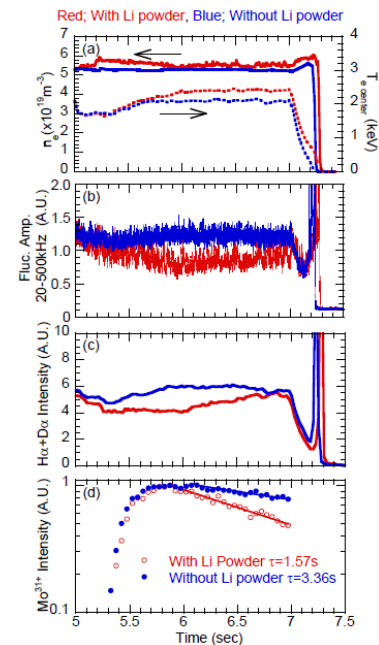


Fig. 2 Effect of Li powder injection. Discharge 189894 with Li powder and discharge 189896 without Li powder. Temporal evolution of (a) \bar{n}_e and $T_e(0)$, (b) line-integrated fluctuation amplitude, (c) H α + D α intensity, and (d) Mo³¹⁺ intensity.

Mo^{31+} is considerably shorter with Li powder, weakening impurity confinement. This effect is beneficial for future fusion reactor operation. Impurity transport analysis revealed comparable diffusion but a weaker inward pinch with Li powder.

Figure 3(a) presents the dependence of \bar{n}_e on ion-scale turbulence levels, as determined by PCI at the normalized position $\rho = 0.5-0.7$. The corresponding experiments were conducted under a constant ECRH heating power of 1.6 MW. The turbulence level decreases with increasing \bar{n}_e up to a specific transition density (n_{tr}) and then increases beyond this point. At n_{tr} , the turbulence phase velocity reverses direction from the ion diamagnetic direction to the electron diamagnetic direction, suggesting a change in turbulence characteristics. The linear growth rate of the ion temperature gradient (ITG) mode (γ_{ITG}), evaluated using a local flux-tube gyrokinetic code, decreases with increasing \bar{n}_e . However, γ_{ITG} does not explain the increase in turbulence levels above n_{tr} . Conversely, the linear growth rate of resistive interchange (RI) turbulence (γ_{RI}), evaluated using a two-fluid magnetohydrodynamics (MHD) code, becomes unstable above n_{tr} . These results indicate that the dominant turbulence mode transitions from drift-wave instability (ITG mode) in the low-density regime to MHD-driven instability (RI mode) in the high-density regime [3].

In the low-density regime, measurements of electron-scale turbulence using backward scattering (BS) revealed the coexistence of local and non-local turbulence characteristics. Typically, when the density or temperature profile changes, turbulence responds on the scale of confinement time. However, ECRH modulation experiments revealed that low-frequency components (10–20 kHz) propagate considerably faster (within 1 ms) than the energy confinement time (~ 40 ms), whereas high-frequency components (50–100 kHz) propagate on the scale of confinement time. The former non-local propagation of low-frequency turbulence becomes evident during the collapse of the internal transport barrier.

In the high-density regime, simultaneous measurements of ion-scale turbulence using Doppler reflectometry and electron-scale turbulence using BS revealed turbulence bifurcation associated with cross-scale interactions. At the bifurcation point, ion-scale turbulence decreased while electron-scale turbulence increased. BS measurements also directly captured changes in the isotropy of turbulence eddies, revealing that the isotropic changes in electron-scale turbulence eddies are a key characteristic of nonlinear interactions. These phenomena are expected to play a crucial role in the formation of the edge transport barrier.

In the low-density plasmas having non-monotonical rotational transform profile under dominant electron heating condition by the NB injection, a large increase in the central ion temperature $T_i(0)$ was observed. This event realized $T_i(0) \sim T_e(0)$. The increase of $T_i(0)$ disappeared in the higher density plasmas. A typical time evolution of $T_i(0)$ is shown in Fig.4(a), where the broken curve indicates the ion temperature with only collisional ion heating by NBI ($P_{i\text{col}}$) of ~ 10 kW/m³. Figure 4 (b) reveals that the amplitude of energetic-ion driven geodesic acoustic mode (EGAM) potential fluctuations measured at $\rho < 0.2$ using heavy ion beam probe is reduced noticeably but sustained at a finite level during the increase phase of $T_i(0)$. The non-collisional ion heating power by the ion Landau damping of EGAM (P_{EGi}) was evaluated by using the observed EGAM potential amplitude, frequency, $T_i(0)$ and the central rotational transform. P_{EGi} clearly exceeded the $P_{i\text{col}}$ during the increase phase of $T_i(0)$ as shown in Fig.4 (c). These findings demonstrate the potential for non-collisional ion heating via resonant interactions between EGAM and thermal ions.

References

- [1] Y. Morishita et al, Sci. Rep. **14**,137 (2024)
- [2] F. Nespoli et al, Nucl. Fusion **63**, 076001 (2023)
- [3] T. Kinoshita et al, Phys. Rev. Lett. **132**, 235101 (2024)

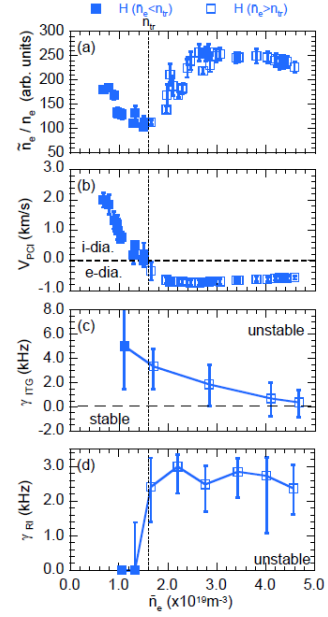


Fig.3 Turbulence transition (a) Turbulence level, (b) turbulence phase velocity, (c) linear growth rate of the ITG mode, and (d) linear growth rate of the RI mode [3].

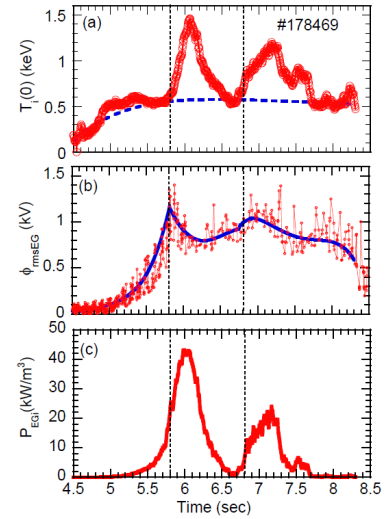


Fig.4 Time evolutions of (a) $T_i(0)$, (b) EGAM potential amplitudes (c) non-collisional ion heating power by the ion Landau damping of EGAM.